SSRG International Journal of Electronics and Communication Engineering
ISSN: 2348-8549/ https://doi.org/10.14445/23488549/IJECE-V12I4P124

Volume 12 Issue 4, 251-264, April 2025

Original Article

Optimized Hyperspectral Vegetation Detection Using Lightweight Cascaded DCNN

Sandhya Shinde[1], Priya Charles[2], Dipak Mahurkar[3], D. Hire[4], Rashmi Deshpande[5]

[1,2,4]*D.Y. Patil International University, Maharashtra, India.*
[3]*Sanjivani College of Engineering, Maharashtra, India.*
[5]*Dr D.Y. Patil Institute of Engineering, Management and Research, Maharashtra, India.*

[1]*Corresponding Author : sandhya.shinde@dypiu.ac.in*

Received: 19 February 2025 Revised: 21 March 2025 Accepted: 20 April 2025 Published: 29 April 2025

Abstract *- Hyperspectral Image Classification (HIC) is essential for distinguishing surface objects and monitoring materials in remote sensing. However, the large number of spectral bands increases computational complexity and classification time. This study proposes a HIC system that uses Deep Convolutional Neural Networks (DCNN) with spectral band selection strategies. The Indian Pines and Salinas datasets are used for evaluation, employing PCA, LDA, and ILDA for band selection. Performance is assessed using accuracy, recall, precision, F1-score, training time, and classification time. The first phase utilizes a three-layered DCNN with PCA for feature representation, achieving 98.20% accuracy on the Indian Pines dataset with 30 spectral bands and a 25×25-pixel window. The second phase introduces a Lightweight Cascaded DCNN (LC-DCNN) with ILDA, enhancing classification accuracy. LC-DCNN+ILDA achieves 99.51% accuracy on Indian Pines and 99.71% on Salinas, outperforming other methods. ILDA proves more effective in selecting discriminative spectral bands than PCA and LDA. In the future, adding bigger datasets with more extensive objects can improve performance for real-time datasets.*

Keywords *- Hyperspectral Image Classification (HIC), Lightweight Cascaded DCNN, Convolutional Neural Network, Principle Component Analysis (PCA), Improved linear discriminant analysis.*

1. Introduction

Ground objects' spectral and spatial representation is obtained using hyperspectral remote sensing technology, which uses the spectrum produced by the objects' distinct composition. The ground items may be recognized and detected, and their quality may be analyzed using hyperspectral images, which also characterize their layout, texture, and shape. The unique physical features and spatial information of the ground objects are represented by the spectral characteristics of the Hyperspectral Images (HSIs) [1, 2]. The HIC is particularly accurate since different materials have different spectrum properties. HSIs are typically used to address issues that natural and multispectral photos are unable to resolve. Numerous applications, including crop observation, precision farming, plant coverage, gas detection, oil spills, land resources, water quality evaluation, and testing on human skin, have therefore made use of hyperspectral pictures [3, 4]. Many scholars have given HSIs a great deal of attention over the last few decades. The three main categories of HIC techniques are spectral, spatial, and spectral-spatial feature methods.

The hyperspectral pictures' salient characteristics are described by the spectral feature approaches using a spectral curve or spectral vector. The spatial feature approaches improve the model's robustness by utilizing the relationship between the core pixel and its context. In the early years, researchers mostly concentrated on the healthy spectral feature technique, which uses logistical regression [7], K-Nearest Neighbor (KNN) [5], and Support Vector Machine (SVM) [6] to classify pixels. Nevertheless, the algorithm's computational complexity is increased by the duplicated information present in the raw spectrum images. Consequently, feature reduction and the most discriminative feature selection techniques, including PCA [8], Independent Component Analysis (ICA) [9], LDA [10], etc., are given increasing attention.

However, this technique's performance is limited since distinct objects may represent the same substance's spectral properties, while different objects may represent different spectral characteristics. Environmental, lighting, atmospheric, and temporal factors all have an impact on the ground objects' inconsistent spectral characteristics. The objects' spatial characteristics provide a wealth of information on the ground objects' layout, shape, and context. Additionally, it gives information about nearby pixels that belong to the same class, which increases the accuracy of classification.

The following is a summary of this article's particular contributions:

- PCA, LDA, and ILDA feature reduction reduces redundant spectral bands to reduce system computing complexity.
- To improve the classification accuracy, The spectral and spatial characteristics of the HSIs are provided by the HIC based on Lightweight Cascaded DCNN (LC-DCNN).

Examining and evaluating suggested approaches using the IP and SD using F1-score, accuracy, recall, and precision. The proposed LC-DCNN+ILDA gives an accuracy of 99.51%, precision of 0.999, recall of 0.995 and F1-score 0.997 for the Indian Pines dataset. It resulted in an accuracy of 99.71%, recall of 99.71, precision of 1.0 and F1-score 1.0 for the Salinas dataset for LC-DCNN+ILDA. It offers a notable enhancement over LC-DCNN+PCA and LC-DCNN+LDA-based spectral band selection.

The subsequent sections of the paper are arranged as follows: Information about earlier research conducted on the HIC is shown in Section 2. A brief description of the supplies and techniques needed to simulate the suggested system is given in Section 3. The HIC experiments conducted on the Indian Pines dataset are discussed in Section 4. Section 5 presents the findings and outlines the potential for further development of the suggested approach.

2. Related Work

Deep learning has gained a lot of interest and advanced quickly during the last 10 years due to its autonomous feature learning capabilities. Because deep learning models can provide joint spectral-spatial information of ground objects, deep learning-based HICs are highly popular. Chen et al. [10] used ensemble-based CNN for HIC in conjunction with transfer learning to speed up the learning process. HIC accuracy has significantly improved when DCNN and ensemble learning are used together.

The datasets from Indian Pines, Salinas, and Pavia University yielded an overall accuracy of 91.20%, 93.35%, and 91.23%, respectively. In order to address the issue of over-smoothing brought on by basic conventional Graph Neural Networks (GNNs), Yao et al. [11] looked at a Deep Hybrid Multi-Graph neural network (DHMG). It reduces the noise in the HSIs and offers improved spectral representation. The overall HIC accuracy for the 2013 Houston, Salinas, and Pavia University datasets was 93.31%, 98.33%, and 97.81%, respectively.

Nevertheless, the spatial and structural information of the objects in HSIs is not provided by GNN-based methods. Consolidated CNN (C-CNN) consists of 2D-CNN to describe abstract spatial features and 3D-CNN to represent spatial spectral data, which was investigated by Chang et al. [12]. The spectral band redundancy elimination process uses the PCA technique, demonstrating a notable increase in classification time. The accuracy of the HIC is enhanced by the data augmentation. The accuracy of C-CNN and C-CNN-Aug on the IP dataset was 73.33% and 83.68%, respectively. In order to reduce computing complexity and increase robustness in the presence of noise, Yuan et al. [13] employed a proxy-based deep learning model. It provides 98.94% and 99.09% accuracy for measures based on similarity and distance, respectively, for the Indian Pines dataset.

The capacity of deep CNN-based techniques to offer a spatial-spectral representation of HSIs makes them appealing. Superpixel Pooling CNN (SP-CNN) [14], Hybrid 2D-3D CNN [15], Sandwich CNN (SFE-SCNN) [17], Deep Attention Graph CNN (DAGCNN) [18], and other DCNN-based techniques are successfully used for the HICs. Unlike PCA, LDA requires class labels and considers both intra- and inter-class variability while reducing dimensions. While PCA gives the maximum number of components equal to the number of features in the dataset, LDA gives the maximum number of components equal to the number of classes minus one.

3. Materials and Methods

3.1. Materials

For the experimental evaluation, two hyperspectral imaging datasets-Indian pines and Salinas-are considered. Due to the limited availability of hyperspectral datasets, numerous studies have utilized between 30% and 70% of the available pixels for training [9, 11, 14]. For training and testing, the hyperspectral patches are divided in a 40:70 ratios.

3.1.1. Indian Pines

The information collected by IVIRIS sensors at the Indian Pines (IP) location in Indiana, USA, is known as the dataset. Each 145 by 145 by 220 spectral band in the HSI images was captured at a different wavelength between 0.4 and 2.5 micrometres. A third of the area is used for agriculture, and the remaining third is covered with natural vegetation and forests. It also has a train line, many low-density housing units, two highway lanes, several small roads, and other man-made structures. Figure 1 shows a number of sample spectral bands extracted from the IPs dataset.

3.1.2. Salinas Dataset

The SD consists of high school photos taken in the Salinas Valley in California. These pictures feature 224 bands and 512 by 217 pixels of resolution. It includes vineyard and vegetable fields and is divided into sixteen categories of uncultivated land.

Figure 1 shows the original IPs and Salinas HSIs, as well as their ground truth band, consisting of information regarding different objects in the HIS.

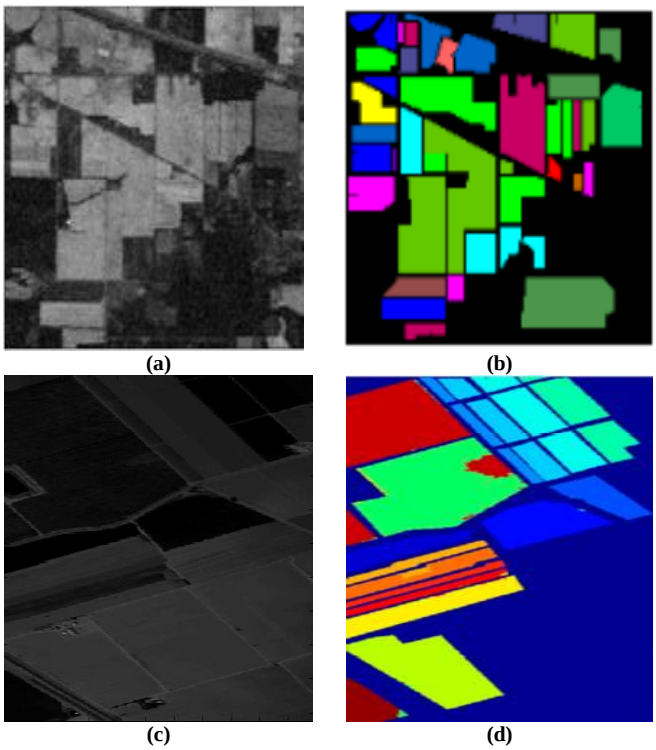

Fig. 1 Dataset details a) IPs image, b) IPs ground truth, c) Salinas image, and d) Salinas ground truth.

The details about the test and training sample of IPs and SD considered for evaluating the proposed methodology are mentioned in the corresponding Tables 1 and 2.

Table 1. Detail about IPs dataset

Sr. No	Hyperspectral Class	Total Samples	Training samples	Testing Samples
1	Alfalfa	46	32	14
2	Corn-notill	1428	1000	428
3	Corn-mintill	830	581	249
4	Corn	237	166	71
5	Grass-pasture	483	338	145
6	Grass-trees	730	511	219
7	Grass-pasture-mowed	28	20	8
8	Hay-windrowed	478	335	143
9	Oats	20	14	6
10	Soybean-notill	972	680	292
11	Soybean-mintill	2455	1719	736
12	Soybean-clean	593	415	178
13	Wheat	205	144	61
14	Woods	1265	886	379
15	Buildings-Grass-Trees-Drives	386	270	116
16	Stone-Steel-Towers	93	65	28
	Total Samples	10249	7176	3073

Table 2. Detail about SD

Sr. No	Hyperspectral Class	Total Samples	Training samples	Testing Samples
1	Brocoli_green_weeds_1	2009	1406	603
2	Brocoli_green_weeds_2	3726	2608	1118
3	Fallow	1976	1383	593
4	Fallow_rough_plow	1394	976	418
5	Fallow_smooth	2678	1875	803
6	Stubble	3959	2771	1188
7	Celery	3579	2505	1074
8	Grapes_untrained	11271	7890	3381
9	Soil_vinyard_develop	6203	4342	1861
10	Corn_senesced_green_weeds	3278	2295	983
11	Lettuce_romaine_4wk	1068	748	320
12	Lettuce_romaine_5wk	1927	1349	578
13	Lettuce_romaine_6wk	916	641	275
14	Lettuce_romaine_7wk	1070	749	321
15	Vinyard_untrained	7268	5088	2180
16	Vinyard_vertical_trellis	1807	1265	542
	Total samples	54129	37891	16238

3.2. Data Preprocessing

Many redundant spectral bands and spectral bands with unnecessary information can be found in the original Indian Pines and Salinas dataset. ILDA aids in analysing the correlation between the HIS's various spectral bands. ILDA's new subspace for multidimensional data exhibits features with substantial variance.

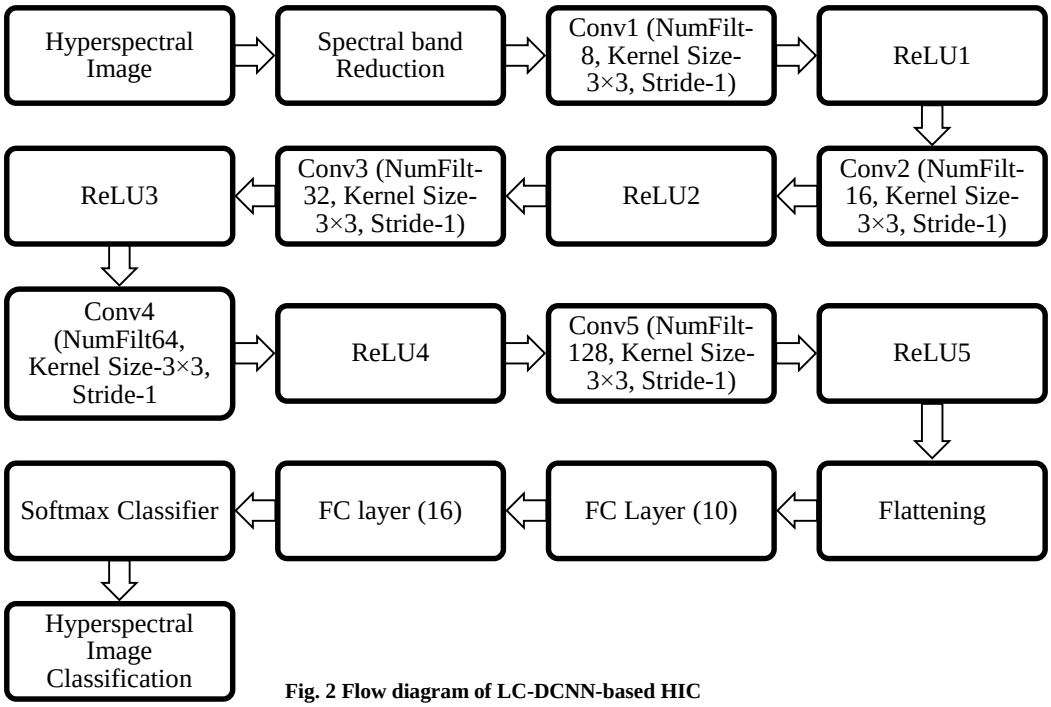

Fig. 2 Flow diagram of LC-DCNN-based HIC

3.3. Proposed Methodology

Figure 2 mentions the suggested HIC's flow diagram. The hyperspectral image with dimensions of 145 x 145 x 220 can be used with the suggested method. Only prominent spectral bands containing significant information are provided by the feature reduction algorithm (PCA/LDA).

The image is separated into a local patch of S×S pixels, and the class of the patch is determined by the class of the center pixel of the local window. In order to prevent confusion in the local window's center pixel, the S is typically taken as an odd integer.

Additionally, the lightweight cascaded CNN is given the patches to learn its spectral and spatial properties. The suggested lightweight cascaded CNN consists of five CNN layers, with the Rectified Linear Unit (ReLU) and Convolution (ConvLayer) layers included in each layer.

Five convolutions, five ReLU, two fully linked, and a classifier layer make up the suggested LC-DCNN architecture. Better local and global feature connectivity of the hyperspectral pictures is made possible by the cascaded structure of the CNN layers.

The filter kernel F is convolved with each Hyperspectral Patch (HSP) to offer the hyperspectral image's local and global information and connectivity. This convolution procedure is provided by Equations 1 and 2. To preserve the original size, the original patch is padded by one pixel around the edge, and the convolution filter is strided by one pixel.

The 3x3 convolution filter F is taken into consideration. It takes into account 8, 16, 32, 64, and 128 filters in each of the five LC-DCNN layers.

$$HSP_{conv}(m,n) = \mathrm{H}SP(m,n) * F(m,n) \quad (1)$$

$$HSP_{conv}(m,n) = \sum_{i=1}^{R}\sum_{j=1}^{C} HSP(i,j)F(i-m,j-n) \quad (2)$$

Where, $HSP_{conv}(m,n)$ represent the hyperspectral image's convolutional map, and F stands for the convolution filter. By substituting 0 for the negative values in equation 3, the ReLU layer reduces linearity and enhances non-linearity. The ReLU layer aids in improving classification and expediting the training process.

$$HSP_{ReLU}(i,j) = \max_{i=1:R,j=1:C}\{0, \mathrm{HSP}_{\mathrm{conv}}(i,j)\} \quad (3)$$

Here, HSP_{ReLU} shows the ReLU layer output. The completely linked layer connects every neuron to every other neuron to increase the deep features' connection and correlation. The classification layer called Softmax is employed to determine a sample's class. The output class is chosen based on the class label with the highest likelihood after the probabilities for each class are provided.

The DCNN algorithm is trained using the Adam optimization method since it has simple computational requirements and requires minimal memory. When an error occurs during the training phase, Adam optimization can automatically modify the learning rate.

The algorithm is trained for 500 epochs, and the learning is done in batches of 64. It took into account decay rates of 0.9 and 0.999, learning rate of 0.001 and positive parameter $\varepsilon = 10^{-8}$ prevent division by zero

4. Experimental Results and Discussion

The proposed LC-DCNN-based HIC system, incorporating PCA, LDA and ILDA for IP and SD, is implemented using MATLAB R2019b on a system equipped with an Nvidia GPU featuring 512 Tensor Cores, 32 GB of RAM, and 16 GB of GPU memory.

Figure 3 shows the ground truth and classification map. The results of the proposed HIC are validated using accuracy, precision, recall, and F1-score, as shown in equations 4 to 7, respectively.

$$Precision = \frac{TP}{TP+FP} \quad (4)$$

$$Recall = \frac{TN}{TN+FN} \quad (5)$$

$$Accuracy(\%) = \frac{TP+TN}{TP+TN+FP+FN} \times 100 \quad (6)$$

$$F1-Score = \frac{2*Precision*Recall}{Precision+Recall} \quad (7)$$

Tables 3 and 4, for the relevant IPs and SDs, indicate the performance of the suggested approach for the PCA, LDA and ILDA feature reduction techniques. Compared to LC-DCNN PCA and LDA, the suggested LC-DCNN and spectral band selection based on ILDA provide superior results.

For the dataset of IPs it offers average accuracy of 98.05%, 99.00% and 99.51% for the LC-DCNN-based HIC for PCA, LDA and ILDA-based spectral band selection, respectively.

For the PCA, LDA and ILDA-based spectral band selection using the LC-DCNN-based HIC, respectively, it provides an average accuracy of 98.62%, 99.63% and 99.71% regarding the SD. Figure 3 shows experimental result visualization. Figure 4-7 shows the result of the accuracy, recall, precision, and F1 score for the IP data set, respectively.

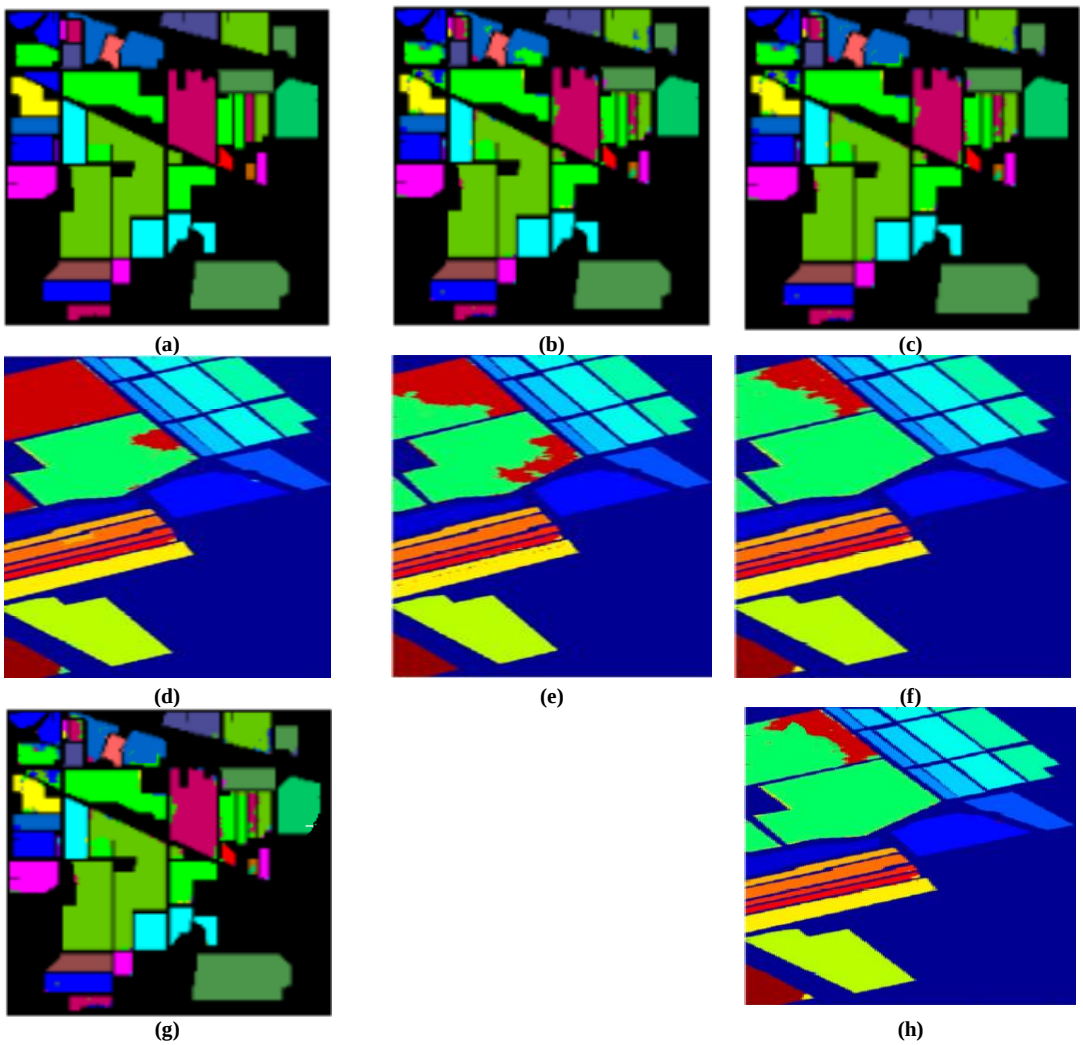

Fig. 3 Experimental results visualization a) & d) the actual situation in IPs and SD b) & e) Classification results using LC-DCNN+PCA for IPs and Salinas c) & f) Classification output using LC-DCNN+LDA for IPs and Salinas g) & h) classification results using LC-DCNN+ILDA for IPs and Salinas

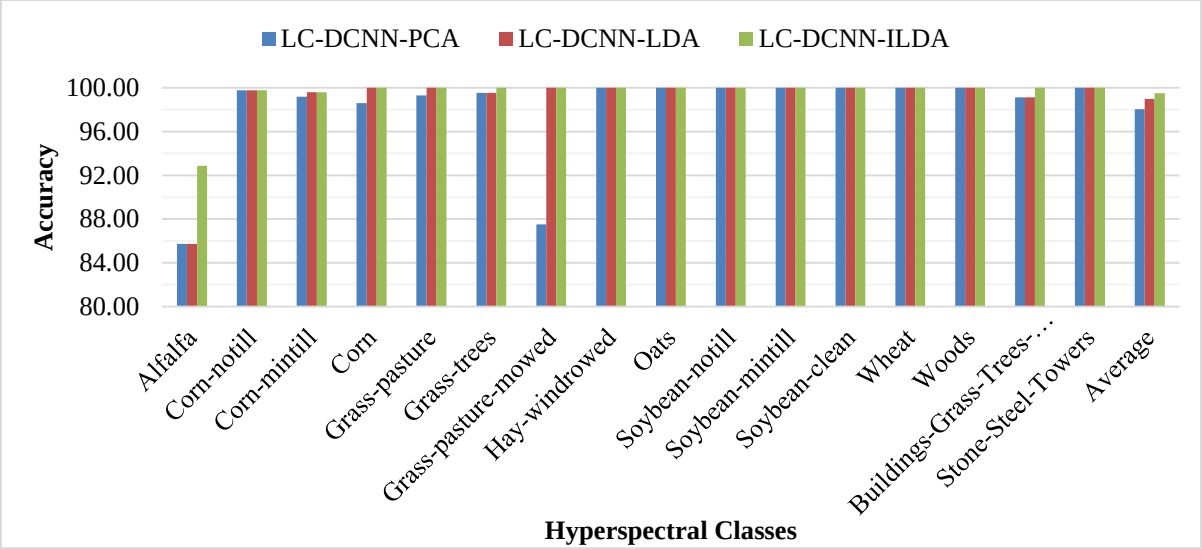

Fig. 4 Accuracy for HIC for IPs dataset

Table 3. Execution of suggested LC-DCNN for various spectral band reduction techniques on IPs dataset

Sr. No	Hyperspectral Class	LC-DCNN+PCA				LC-DCNN+LDA				LC-DCNN+ILDA			
		Accuracy	Recall	Precision	F1-Score	Accuracy	Recall	Precision	F1-Score	Accuracy	Recall	Precision	F1-Score
1	Alfalfa	85.71	0.86	1	0.923	85.7	0.857	1	0.923	92.86	0.929	1	0.963
2	Corn-notill	99.77	1	1	0.998	99.8	0.998	1	0.999	99.77	0.998	1	0.999
3	Corn-mintill	99.20	0.99	1	0.996	99.6	0.996	1	0.998	99.6	0.996	1	0.998
4	Corn	98.59	0.99	1	0.993	100	1	1	1	100	1	1	1
5	Grass-pasture	99.31	0.99	0.99	0.993	100	1	1	1	100	1	1	1
6	Grass-trees	99.54	1	1	0.995	99.5	0.995	1	0.998	100	1	1	1
7	Grass-pasture-mowed	87.50	0.88	1	0.933	100	1	1	1	100	1	1	1
8	Hay-windrowed	100.00	1	0.99	0.997	100	1	0.993	0.997	100	1	0.993	0.997
9	Oats	100.00	1	1	1	100	1	1	1	100	1	1	1
10	Soybean-notill	100.00	1	0.99	0.997	100	1	0.993	0.997	100	1	0.997	0.998
11	Soybean-mintill	100.00	1	1	0.999	100	1	0.999	0.999	100	1	1	1
12	Soybean-clean	100.00	1	1	1	100	1	1	1	100	1	1	1
13	Wheat	100.00	1	0.98	0.992	100	1	0.984	0.992	100	1	1	1
14	Woods	100.00	1	0.99	0.997	100	1	0.997	0.999	100	1	0.997	0.999
15	Buildings-Grass-Trees-Drives	99.14	0.99	1	0.996	99.1	0.991	1	0.996	100	1	1	1
16	Stone-Steel-Towers	100.00	1	1	1	100	1	1	1	100	1	1	1
Average		**98.05**	0.98	1	0.989	**99**	0.99	0.998	0.994	**99.51**	0.995	0.999	0.997

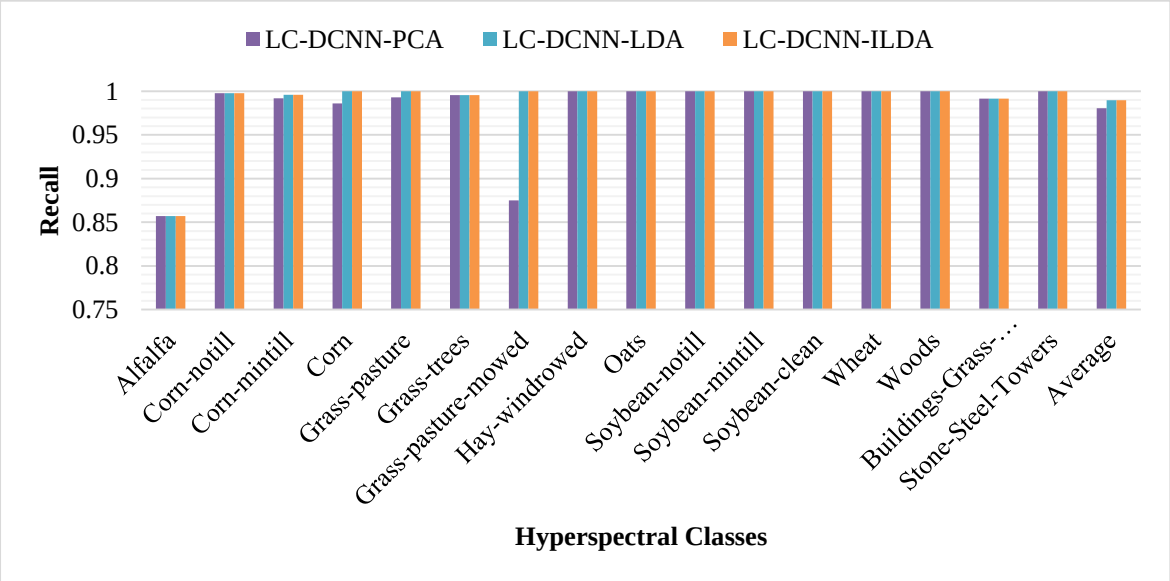

Fig. 5 Recall for HIC for IPs dataset

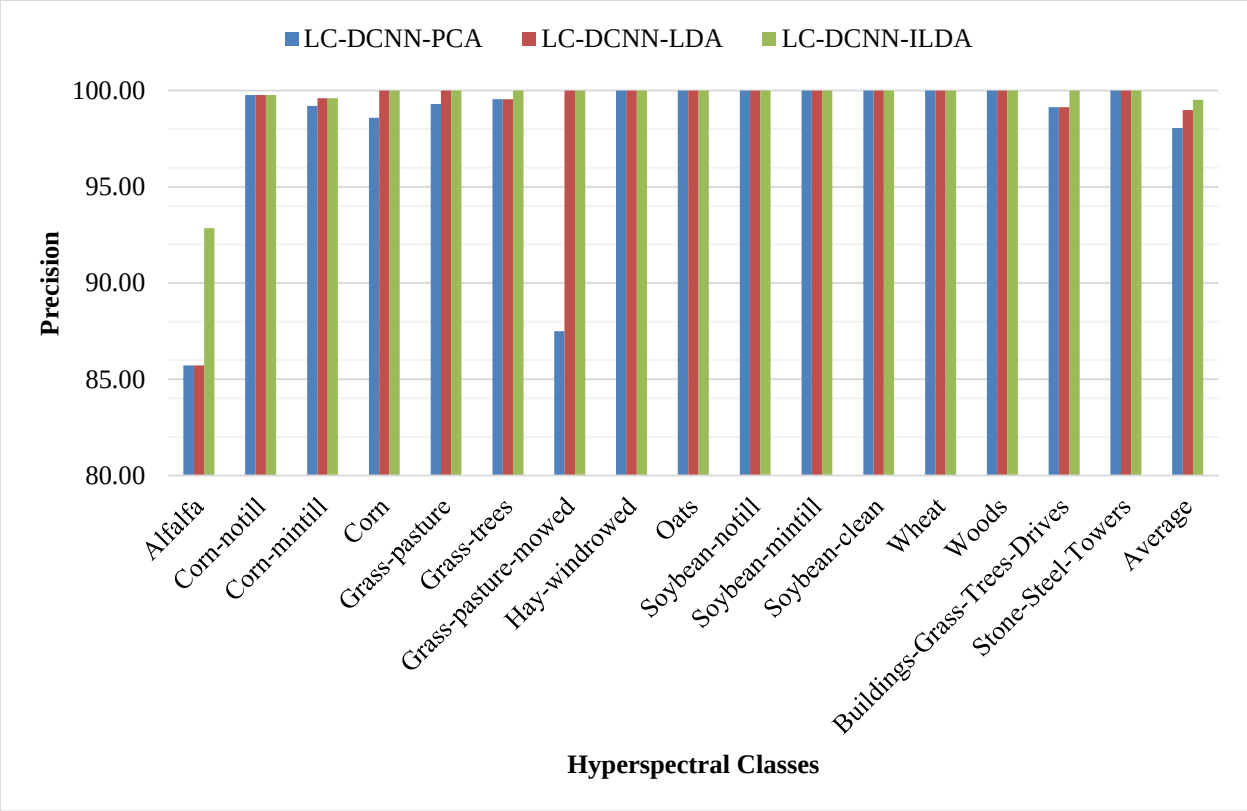

Fig. 6 Precision for HIC for IPs dataset

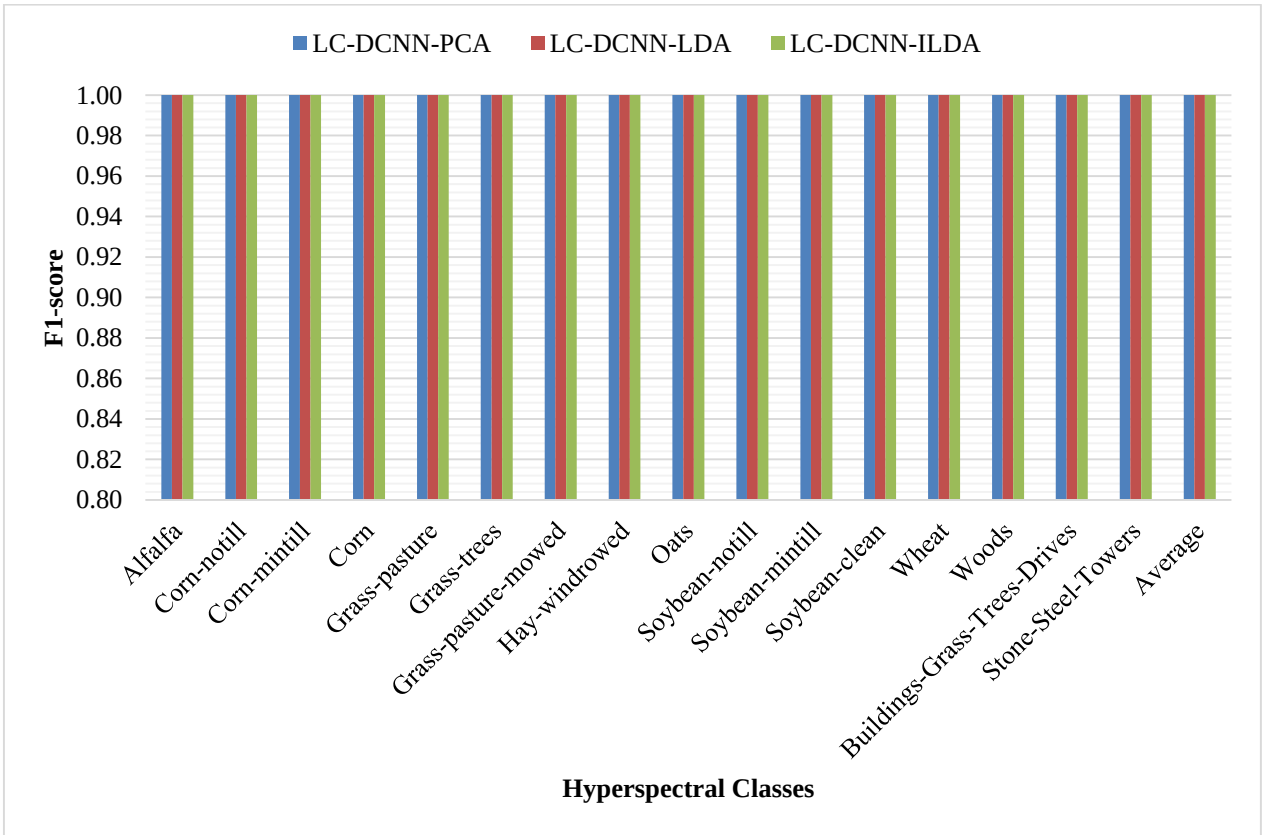

Fig. 7 F1-score for HIC for IPs dataset

Table 4. Performance of suggested LC-DCNN for various spectral band reduction techniques on SD

Sr. No	Hyperspectral Class	LC-DCNN+PCA				LC-DCNN+LDA				LC-DCNN+ILDA			
		Accuracy	Recall	Precision	F1-Score	Accuracy	Recall	Precision	F1-Score	Accuracy	Recall	Precision	F1-Score
1	Brocoli_green_weeds_1	98.67	0.99	0.99	0.987	99.3	0.993	0.993	0.993	99.67	1.00	0.99	1.00
2	Brocoli_green_weeds_2	99.82	1	1	0.997	100	1	0.996	0.998	100.00	1.00	1.00	1.00
3	Fallow	99.33	0.99	0.98	0.988	99.3	0.993	0.997	0.995	99.33	0.99	1.00	0.99
4	Fallow_rough_plow	98.56	0.99	0.99	0.988	99.8	0.998	0.998	0.998	99.76	1.00	1.00	1.00
5	Fallow_smooth	99.00	0.99	1	0.994	99.8	0.998	0.998	0.998	99.75	1.00	1.00	1.00
6	Stubble	99.24	0.99	0.99	0.992	99.2	0.992	0.999	0.996	99.24	0.99	1.00	1.00
7	Celery	99.23	0.99	1	0.994	99.2	0.992	1	0.996	99.49	0.99	1.00	1.00
8	Grapes_untrained	99.38	0.99	1	0.996	100	1	0.999	1	100.00	1.00	1.00	1.00
9	Soil_vinyard_develop	99.19	0.99	1	0.995	99.2	0.992	0.999	0.996	99.57	1.00	1.00	1.00
10	Corn_senesced_green_weeds	99.69	1	0.98	0.99	99.7	0.997	0.998	0.997	99.69	1.00	1.00	1.00
11	Lettuce_romaine_4wk	99.38	0.99	0.96	0.978	100	1	0.985	0.992	100.00	1.00	0.99	1.00
12	Lettuce_romaine_5wk	99.13	0.99	0.98	0.985	99.1	0.991	0.998	0.995	99.48	0.99	1.00	1.00
13	Lettuce_romaine_6wk	90.18	0.9	0.97	0.936	99.6	0.996	0.986	0.991	99.64	1.00	0.99	0.99
14	Lettuce_romaine_7wk	98.13	0.98	0.96	0.971	100	1	0.979	0.989	100.00	1.00	0.98	0.99
15	Vinyard_untrained	99.77	1	1	0.997	100	1	0.996	0.998	100.00	1.00	1.00	1.00
16	Vinyard_vertical_trellis	99.26	0.99	0.99	0.989	99.8	0.998	0.985	0.992	99.82	1.00	0.99	0.99
Average		98.62	0.99	0.99	0.986	99.6	0.996	0.994	0.995	99.71	99.71	1.00	1.00

The graphical representation of the various performance metrics for the HIC for Table 5 shows the SD, respectively. It is noted that the suggested LC-DCNN+ILDA provides better overall accuracy compared with LC-DCNN+LDA and LC-DCNN+PCA for SD. The HIC's qualitative and quantitative findings are superior for LC-DCNN+ILDA compared with LC-DCNN+LDA and LC-DCNN+PCA. The lower intra-class variance and maximum interclass variance considerations during the selection of spectral bands in the ILDA algorithm provide superiority over the LDA and PCA-based spectral band selections. The outcomes of the HIC based on LC-DCNN are examined across varying patch sizes and spectral bands. The effects of the different number of spectral bands created using PCA, LDA and ILDA on the performance of the HIC for a patch size of 25*25 pixels are shown in Figure 8 and 9. It has been found that for 30 spectral bands, the suggested approach performs better. It gives 98.05%, 99.00% and 99.51% accuracy for HIC using proposed LC-DCNN using PCA, LDA and ILDA with 30 spectral bands, respectively, for the IPs dataset. It results in 98.62%, 99.63% and 99.71% accuracy for HIC using proposed LC-DCNN using PCA LDA, and ILDA correspondingly for 30 SD spectral bands. Reduced spectral band count results in insufficient spectral representation, whereas a bigger number of spectral bands increases the disparity of spectral characteristics within and across classes.

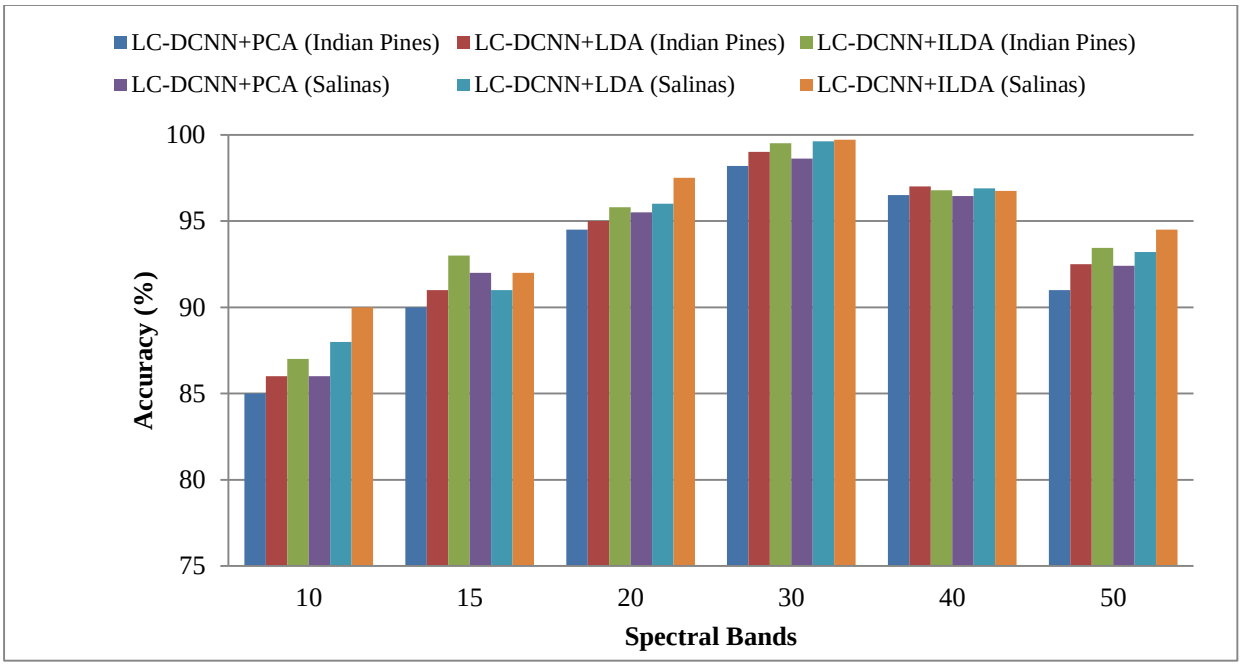

Fig. 8 Performance of the suggested system for various spectral band counts

For 30 spectral bands chosen using PCA, LDA and ILDA, Figure 12 shows the impact of patch size variation on the proposed HIC scheme's performance. It provided 99.51% and 99.71% accuracy for LC-DCNN+ILDA for Indian Pines and

Salinas dataset. In comparison to patches of larger and smaller sizes, a patch size of 25*25 shows a stronger connectedness of the local area and particular class of the HIS. As shown in Table 5, the effectiveness of the suggested strategy is contrasted with earlier methods used for the HIC on the IPs and SD. It has been noted that the LDA's class-wise discrimination aids in the discriminative spectral bands' selection.

The average recognition time per sample is 36 sec, 38 sec and 38 sec for LC-DCNN+PCA, LC-DCNN+LDA and LC-DCNN+ILDA based HIC, respectively, for the IPs dataset. The average recognition time per sample is 55 sec, 62 sec and 60 sec for LC-DCNN+PCA, LC-DCNN+LDA and LC-DCNN+ILDA-based HIC, respectively, for the SP dataset.

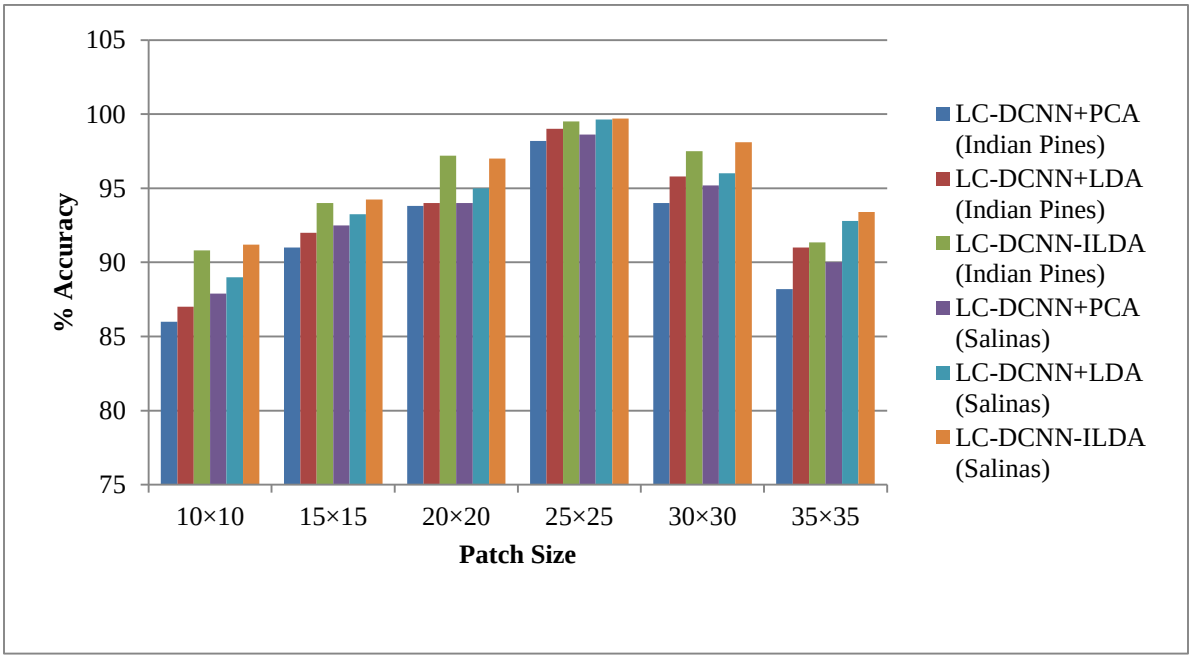

Fig. 9 Accuracy percentages of the suggested methods for various spectral patch sizes

Table 5. Performance evaluation in relation to earlier artistic states

Author and Year	Method	Indian Pines		Salinas	
		Accuracy (%)	Recognition Time (s)	Accuracy (%)	Recognition Time (s)
Chen et al. (2019)	Deep CNN-Ensemble	91.20	38s	96.88	183s
Chang et al. (2022)	C-CNN	83.68	39s	99.43	111s
Xie et al. (2021)	SP-CNN-8	93.57	880s	96.12	-
Gao et al. (2021)	SFE-SCNN	98.72	-	99.56	-
Bai et al. (2022)	DAGCNN	98.61	-	-	-
Shinde and Patidar (2022)	DCNN	98.20%	36s	-	-
Proposed Method	LC-DCNN+PCA	98.05	36s	98.62	55s
	LC-DCNN+LDA	99.00	38s	99.63	62s
	LC-DCNN+ILDA	99.51	38s	99.71	60s

Figures 10 and 11 illustrate the agreement between the suggested scheme's accuracy and the prior state of the art. The Deep CNN ensemble [10], C-CNN [19], SP-CNN-8 [14], SPE-CNN [17], DAGCNN [18], and DCNN provided an accuracy of 91.20%, 83.68%, 93.57%, 98.72%, 98.61%, and 98.20% respectively for IPs dataset. However, proposed LC-DCNN provides 98.05%, 99%, and 99.51% accuracy for the IPs dataset's PCA, LDA and ILDA-based spectral band reduction. The Deep CNN ensemble, C-CNN, SP-CNN-8, and SPE-CNN have given accuracy of 96.88%, 99.43%, 96.12%, and 99.56%, respectively, for SD. However, the proposed LC-DCNN provides 98.62%, 99.63% and 99.71% accuracy for PCA, LDA and ILDA-based spectral band reduction for SD.

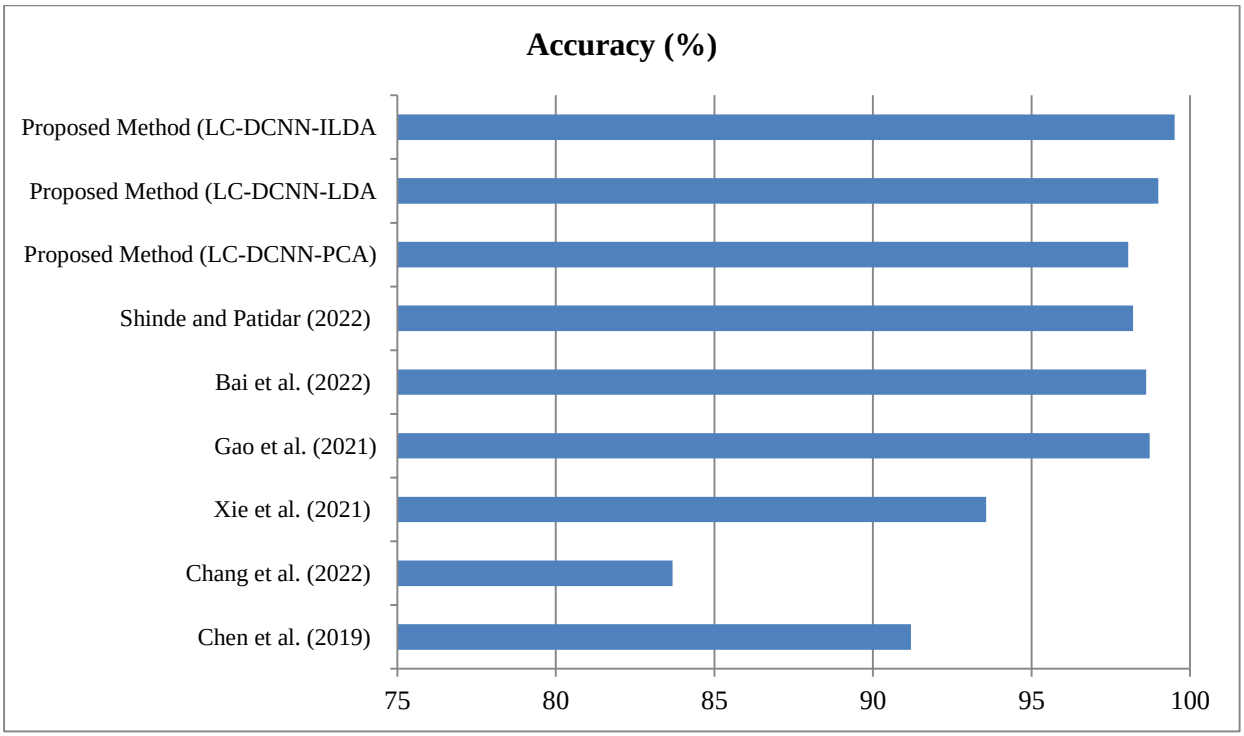

Fig. 10 Accuracy comparison with the previous state of arts (IPs Dataset)

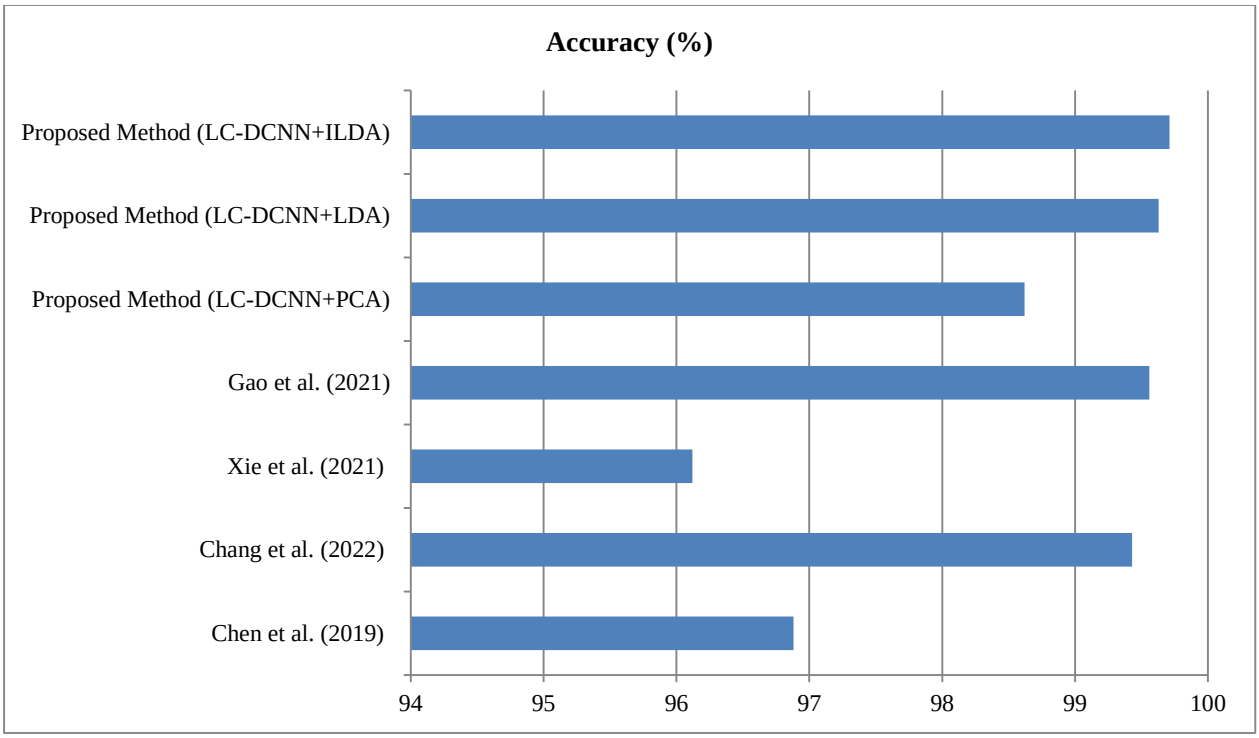

Fig. 11 Accuracy comparison with the previous state of arts (SD)

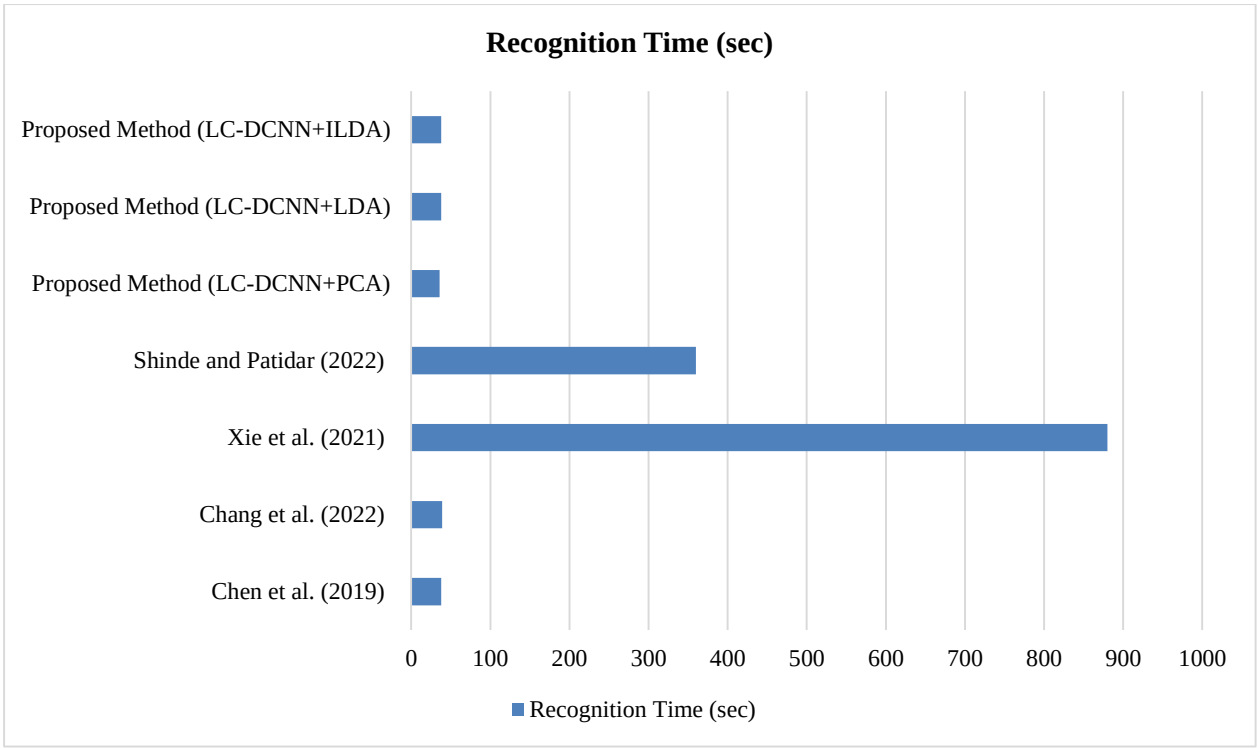

Fig. 12 Recognition time comparison with the previous state of arts (IPs Dataset)

When the performance of the recognition time of the LC-DCNN is compared with the previous state of arts, it shows 36sec, 38sec and 38sec sec recognition time for the LC-DCNN+PCA, LC-DCNN+LDA and LC-DCNN+ILDA, respectively, for IPs dataset showed in figure 12. However, the previous methods, such as deep CNN ensemble and C-CNN, provide the recognition time of 110 sec and 188 sec, respectively. The presented LC-DCNN provides lower trainable parameters compared with previous schemes and reduces the system's recognition time as much as possible.

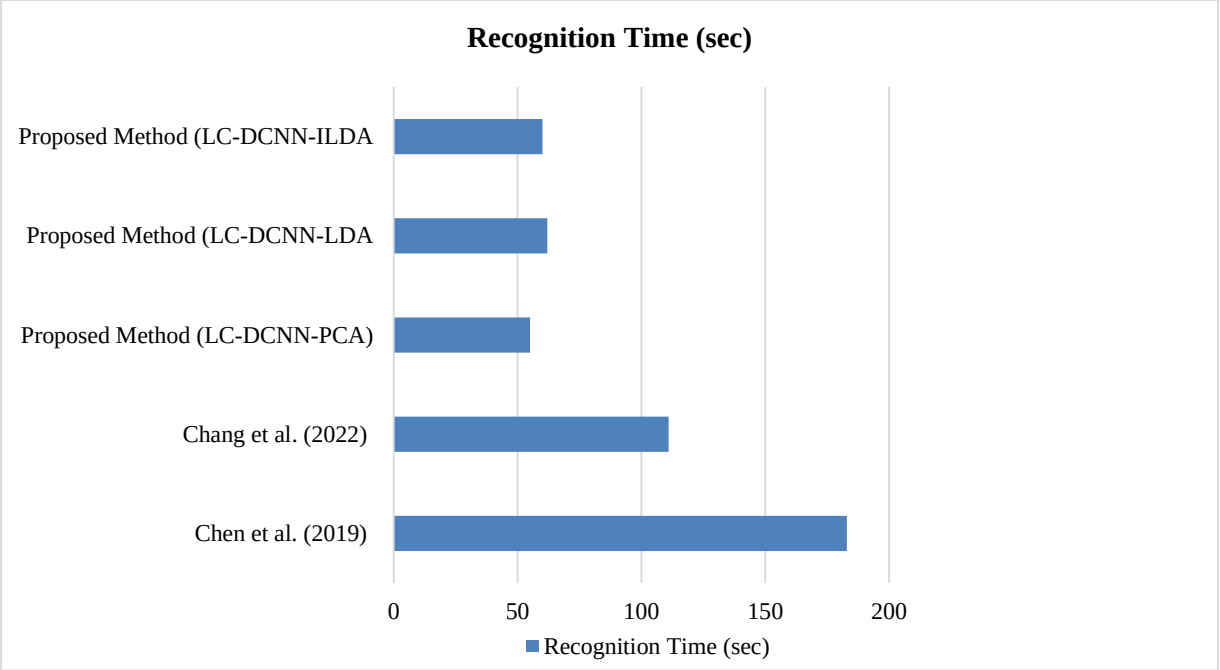

Fig. 13 Recognition time comparison with the previous state of arts (SD)

When the performance of the recognition time of the LCDCNN is compared with the previous state of arts, it shows 55 sec, 62 sec and 60 sec recognition time for the LC-DCNN+PCA, LC-DCNN+LDA and LC-DCNN+ILDA respectively, for SD in Figure 13. However, the previous methods, such as deep CNN ensemble and C-CNN, provide a recognition time of 110 sec and 188 sec, respectively. The presented LC-DCNN provides lower trainable parameters compared with previous schemes that reduce the system's recognition time as much as possible.

5. Conclusion

Thus, this chapter introduces the lightweight HIC based on Cascaded Convolutional Neural Networks. It facilitates the characterization of the HS images' spectral and spatial properties. The lightweight design reduces the complexity and time required for calculations. The evaluation outcome of the proposed LC-DCNN is investigated using a number of feature selection techniques, such as PCA, LDA, and ILDA. It evaluates the performance of the suggested approach for 16 distinct class classifications using the IPs dataset. Overall accuracy in the IPs dataset is 99.51% for LC-DCNN-ILDA, 99% for LC-DCNN+LDA, and 98.05% for LC-DCNN+PCA.

However, the overall accuracy of LC-DCNN-ILDA, LC-DCNN+LDA, and LC-DCNN+PCA in the SD is 99.71%, 99.63%, and 98.62%, respectively. It is clear that the suggested LC-DCNN+ILDA system provides higher classification accuracy when compared to the traditional state-of-the-art methods used by the HIC. The suggested approach may be applied in the future to a number of tasks, including the analysis of agricultural production, the identification of plant leaf diseases, the detection of marine objects, and wild monitoring.

References

[1] Maryam Imani, and Hassan Ghassemian, "An Overview on Spectral and Spatial Information Fusion for Hyperspectral Image Classification: Current Trends and Challenges," *Information Fusion*, vol. 59, pp. 59-83, 2020. [CrossRef] [Google Scholar] [Publisher Link]

[2] Wenjing Lv, and Xiaofei Wang, "Overview of Hyperspectral Image Classification," *Journal of Sensors*, vol. 2020, pp. 1-13, 2020. [CrossRef] [Google Scholar] [Publisher Link]

[3] Sen Jia et al., "A Survey: Deep Learning for Hyperspectral Image Classification with Few Labeled Samples," *Neurocomputing*, vol. 448, pp. 179-204, 2021. [CrossRef] [Google Scholar] [Publisher Link]

[4] Gizem Ortac, and Giyasettin Ozcan, "Comparative Study of Hyperspectral Image Classification by Multidimensional Convolutional Neural Network Approaches to Improve Accuracy," *Expert Systems with Applications*, vol. 182, 2021. [CrossRef] [Google Scholar] [Publisher Link]

[5] Bing Tu et al., "KNN-Based Representation of Superpixels for Hyperspectral Image Classification," *IEEE Journal of Selected Topics in Applied Earth Observations and Remote Sensing*, vol. 11, no. 11, pp. 4032-4047, 2018. [CrossRef] [Google Scholar] [Publisher Link]

[6] Yanhui Guo et al., "Hyperspectral Image Classification with SVM and Guided Filter," *EURASIP Journal on Wireless Communications and Networking*, vol. 2019, pp. 1-9, 2019. [CrossRef] [Google Scholar] [Publisher Link]

[7] Jianwei Zheng et al., "Hyperspectral Image Classification Using Mixed Convolutions and Covariance Pooling," *IEEE Transactions on Geoscience and Remote Sensing*, vol. 59, no. 1, pp. 522-534, 2021. [CrossRef] [Google Scholar] [Publisher Link]

[8] A. Villa et al., "Independent Component Discriminant Analysis for Hyperspectral Image Classification," *2nd Workshop on Hyperspectral Image and Signal Processing: Evolution in Remote Sensing*, Reykjavik, Iceland, pp. 4865-4876, 2010. [CrossRef] [Google Scholar] [Publisher Link]

[9] Chao Xia et al., "Maize Seed Classification Using Hyperspectral Image Coupled with Multi-Linear Discriminant Analysis," *Infrared Physics & Technology*, vol. 103, 2019. [CrossRef] [Google Scholar] [Publisher Link]

[10] Yushi Chen et al., "Deep Learning Ensemble for Hyperspectral Image Classification," *IEEE Journal of Selected Topics in Applied Earth Observations and Remote Sensing*, vol. 12, no. 6, pp. 1882-1897, 2019. [CrossRef] [Google Scholar] [Publisher Link]

[11] Ding Yao et al., "Deep Hybrid: Multi-Graph Neural Network Collaboration for Hyperspectral Image Classificatio," *Defence Technology*, vol. 23, pp. 164-176, 2023. [CrossRef] [Google Scholar] [Publisher Link]

[12] Yang-Lang Chang et al., "Consolidated Convolutional Neural Network for Hyperspectral Image Classification," *Remote Sensing*, vol. 14, no. 7, pp. 1-16, 2022. [CrossRef] [Google Scholar] [Publisher Link]

[13] Yuan Yuan, Chengze Wang, and Zhiyu Jiang, "Proxy-Based Deep Learning Framework for Spectral–Spatial Hyperspectral Image Classification: Efficient and Robust," *IEEE Transactions on Geoscience and Remote Sensing*, vol. 60, pp. 1-15, 2022. [CrossRef] [Google Scholar] [Publisher Link]

[14] Fuding Xie et al., "Hyperspectral Image Classification Based on Superpixel Pooling Convolutional Neural Network with Transfer Learning," *Remote Sensing*, vol. 13, no. 5, pp. 1-16, 2021. [CrossRef] [Google Scholar] [Publisher Link]

[15] Alou Diakite, Gui Jiangsheng, and Fu Xiaping, "Hyperspectral Image Classification Using 3D 2D CNN," *IET Image Processing*, vol. 15, no. 5, pp. 1083-1092, 2021. [CrossRef] [Google Scholar] [Publisher Link]

[16] Saeed Ghaderizadeh et al., "Hyperspectral Image Classification Using a Hybrid 3D-2D Convolutional Neural Networks," *IEEE Journal of Selected Topics in Applied Earth Observations and Remote Sensing*, vol. 14, pp. 7570-7588, 2021. [CrossRef] [Google Scholar] [Publisher Link]

[17] Hongmin Gao, Zhonghao Chen, and Chenming Li, "Sandwich Convolutional Neural Network for Hyperspectral Image Classification Using Spectral Feature Enhancement," *IEEE Journal of Selected Topics in Applied Earth Observations and Remote Sensing*, vol. 14, pp. 3006-3015, 2021. [CrossRef] [Google Scholar] [Publisher Link]

[18] Jing Bai et al., "Hyperspectral Image Classification Based on Deep Attention Graph Convolutional Network," *IEEE Transactions on Geoscience and Remote Sensing*, vol. 60, pp. 1-16, 2022. [CrossRef] [Google Scholar] [Publisher Link]

[19] Yang-Lang Chang et al., "Consolidated Convolutional Neural Network for Hyperspectral Image Classification," *Remote Sensing*, vol. 14, no. 7, pp. 1-16, 2022. [CrossRef] [Google Scholar] [Publisher Link]